Supporting Information

Enhanced magnetic susceptibility in $Ti_3C_2T_x$ MXene with Co and Ni metal incorporation

Yizhou Yang,[1,†] Mark Anayee,[1,2,†] Ajith Pattammattel,[3] Mikhail Shekhirev,[1,2] Ruocun (John) Wang,[1,2] Xiaojing Huang,[3] Yong S. Chu,[3] Yury Gogotsi,[1,2] Steven J. May[1]

[1] Department of Materials Science and Engineering, Drexel University, Philadelphia, Pennsylvania 19014, USA

[2] A.J. Drexel Nanomaterials Institute, Drexel University, Philadelphia, Pennsylvania 19104, USA

[3] Brookhaven National Laboratory, National Synchrotron Light Source II, Upton, New York 11973, USA

† These authors contributed equally to the work.

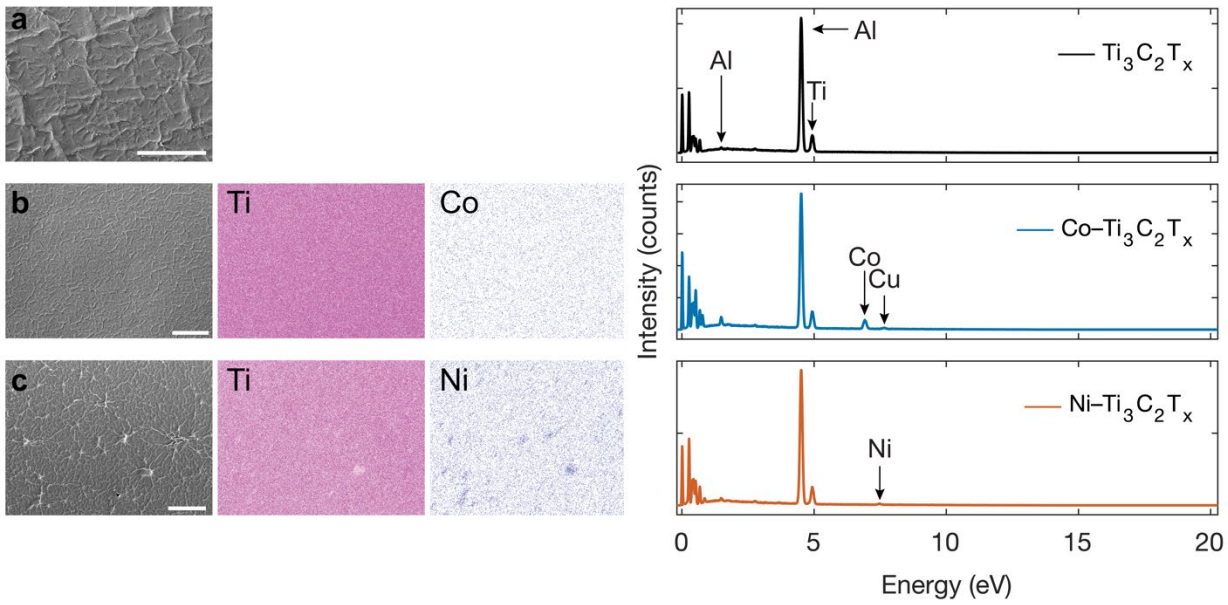

Figure S1. Scanning electron microscopy (SEM) images and corresponding energy dispersive spectroscopy (EDS) maps of Ti, Co, and Ni for (a) pristine, and (b) Co and (c) Ni incorporated $Ti_3C_2T_x$ MXene free-standing films

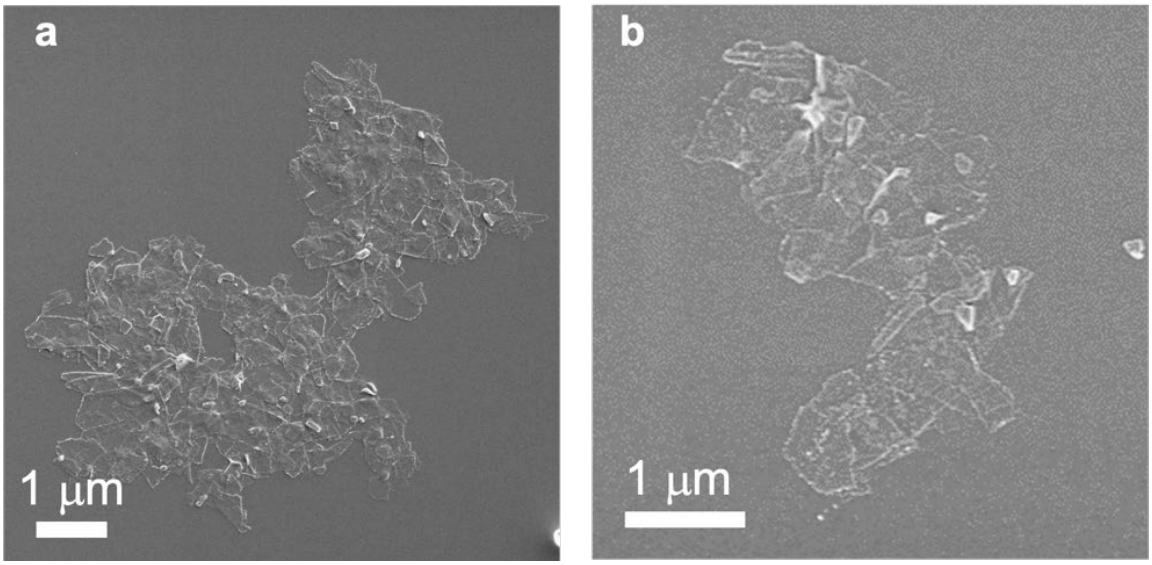

Figure S2. Scanning electron microscopy (SEM) images of drop-cast (a) Co and (b) Ni incorporated $Ti_3C_2T_x$ MXene samples on Si substrates, which were used for XRF analysis.

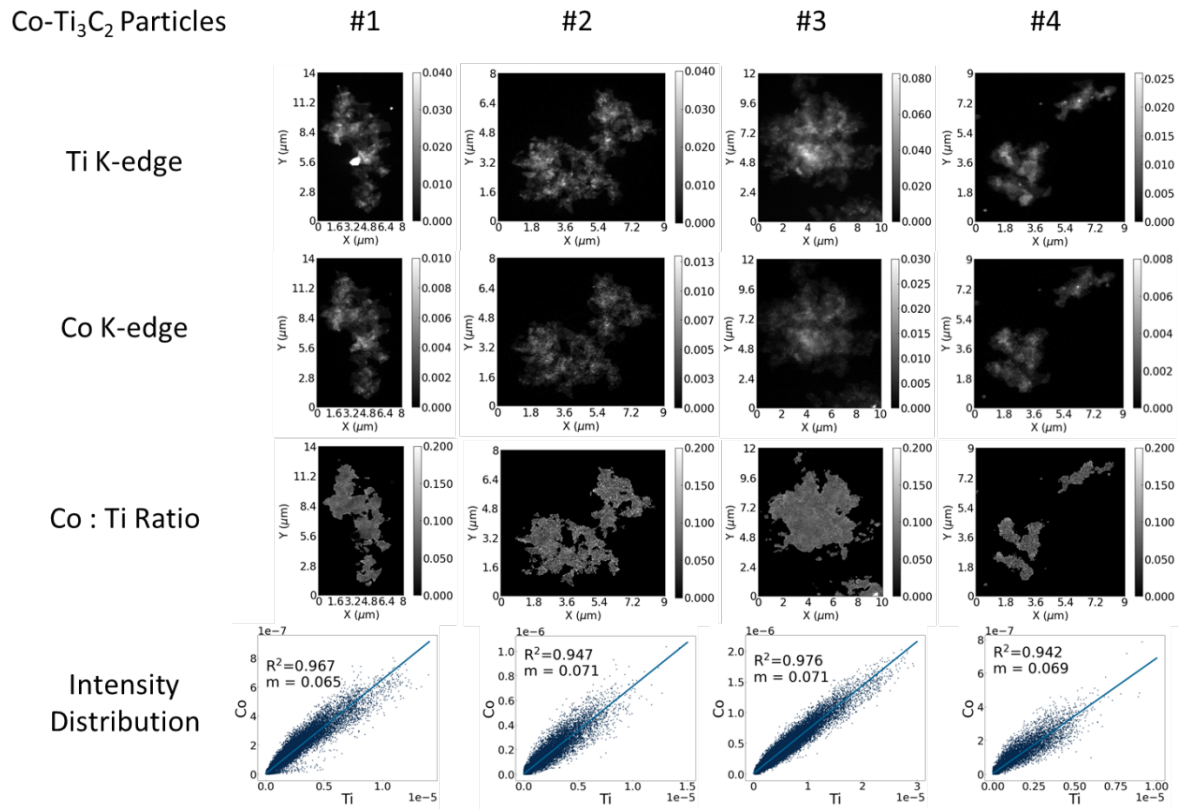

Figure S3. Nano XRF images and element distribution maps for four different Co-$Ti_3C_2T_x$ samples revealing sample-to-sample uniformity.

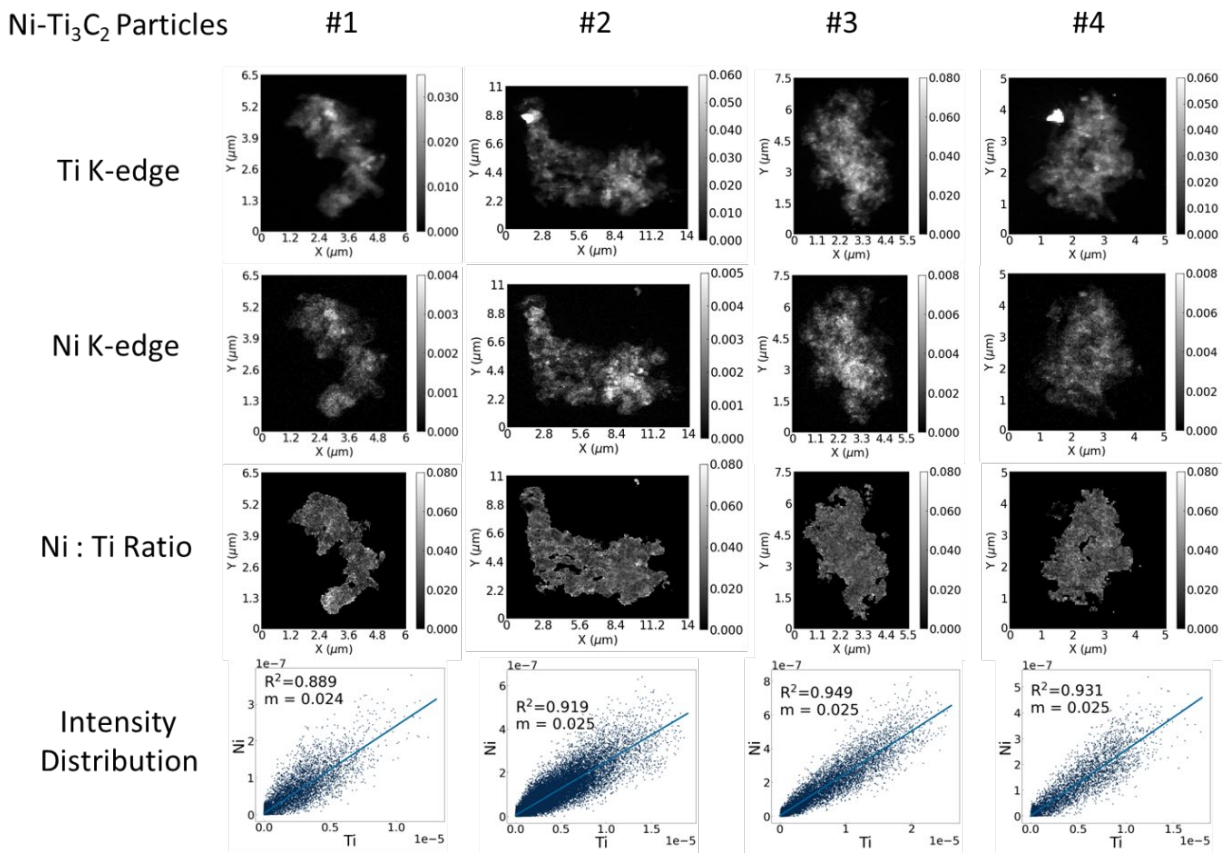

Figure S4. Nano XRF images and element distribution maps for four different Ni-$Ti_3C_2T_x$ samples, revealing sample-to-sample uniformity.

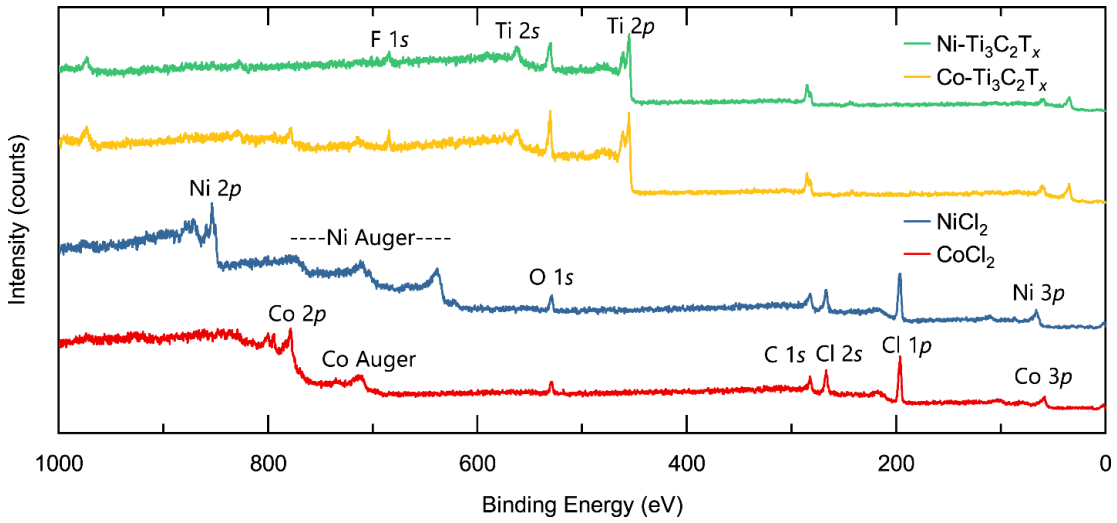

Figure S5. XPS survey spectra for the Co and Ni incorporated $Ti_3C_2T_x$ MXene free-standing films, and $NiCl_2$ and $CoCl_2$ salt powders.

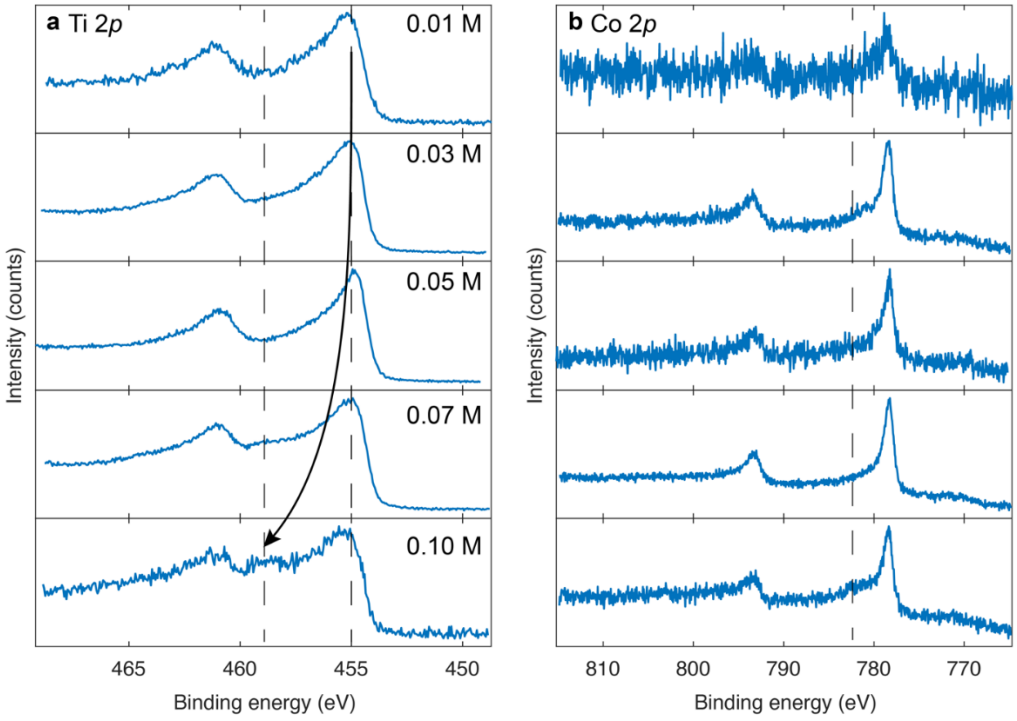

Figure S6. (a) Ti 2*p* and (b) Co 2*p* XPS spectra for Co incorporated $Ti_3C_2T_x$ MXene free-standing films prepared by mixing MXene dispersions with different concentrations of $CoCl_2$ salt. The arrow and dashed line in (a) highlight the shift in spectral features attributed to the increasing oxidation of the Ti. The dashed line in (b) highlights the shift toward higher binding energy and possible oxidation of Co.

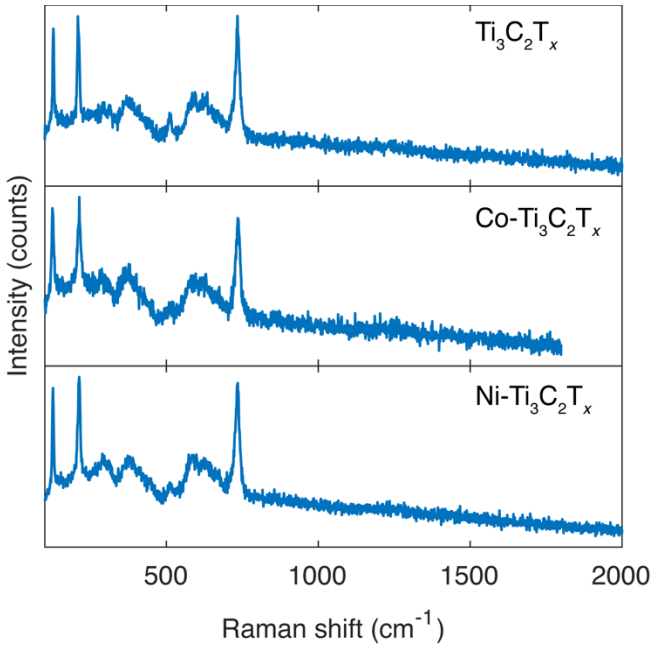

Figure S7. Raman spectra of *d*-$Ti_3C_2T_x$, Co-$Ti_3C_2T_x$, and Ni-$Ti_3C_2T_x$.

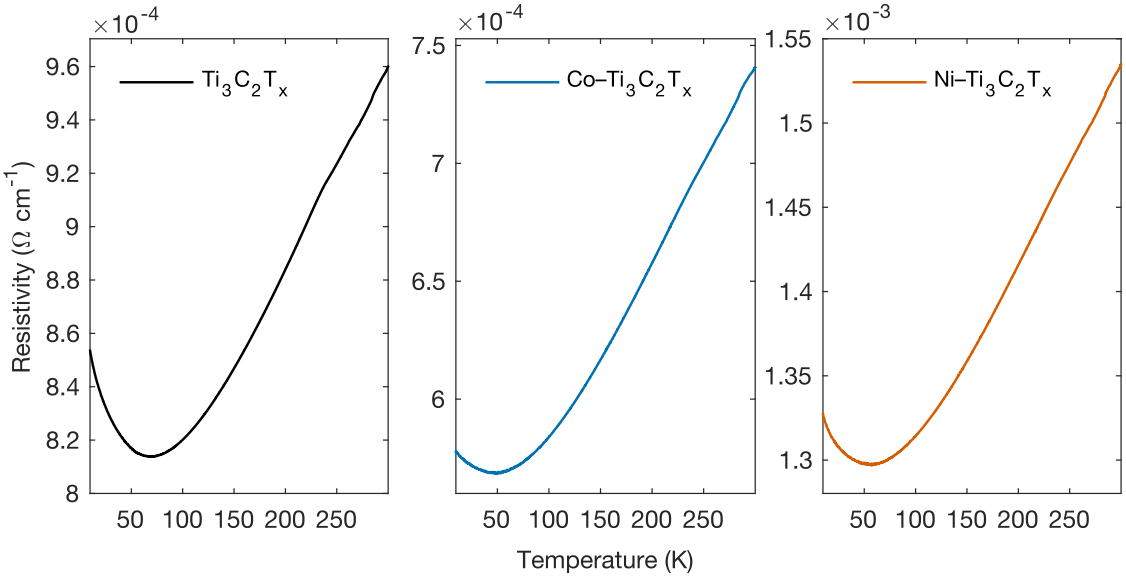

Figure S8. Temperature dependent resistivity measurements of $Ti_3C_2T_x$ MXene free-standing films before and after Co and Ni metal incorporation.

DC magnetization measurements

The DC magnetization was measured by vibrating sample magnetometry (VSM) with a Physical Property Measurement System (PPMS, Quantum Design). All measurements were done in powder form in a plastic sample holder. The free-standing films were broken into small pieces and then loaded into the sample holder. The sample masses were 24.5, 10.0, and 6.9 mg for pristine, and Co and Ni incorporated $Ti_3C_2T_x$ MXene.

The low-temperature magnetization measured in Co and Ni incorporated samples can be fit with a Langevin function,

$$M(H) = A * \left\{\left[Coth\left(\frac{B*H}{k_bT}\right) - \frac{k_bT}{B*H}\right] + C * H\right\}.$$[58-60]

When this function is used to fit behavior arising from non-interacting magnetic particles, such as a superparamagnetic state, *A* is related to the number of independent magnetic clusters, *B* represents the saturation magnetization which is temperature dependent, and *C* is the paramagnetic background of the sample. Constant *A* is fixed for each sample since the Co and Ni concentration is temperature independent. Fitting results for Co incorporated MXene indicate that both *B* and *C* decrease with increasing temperature (**Figure S9** and **Table S1**).

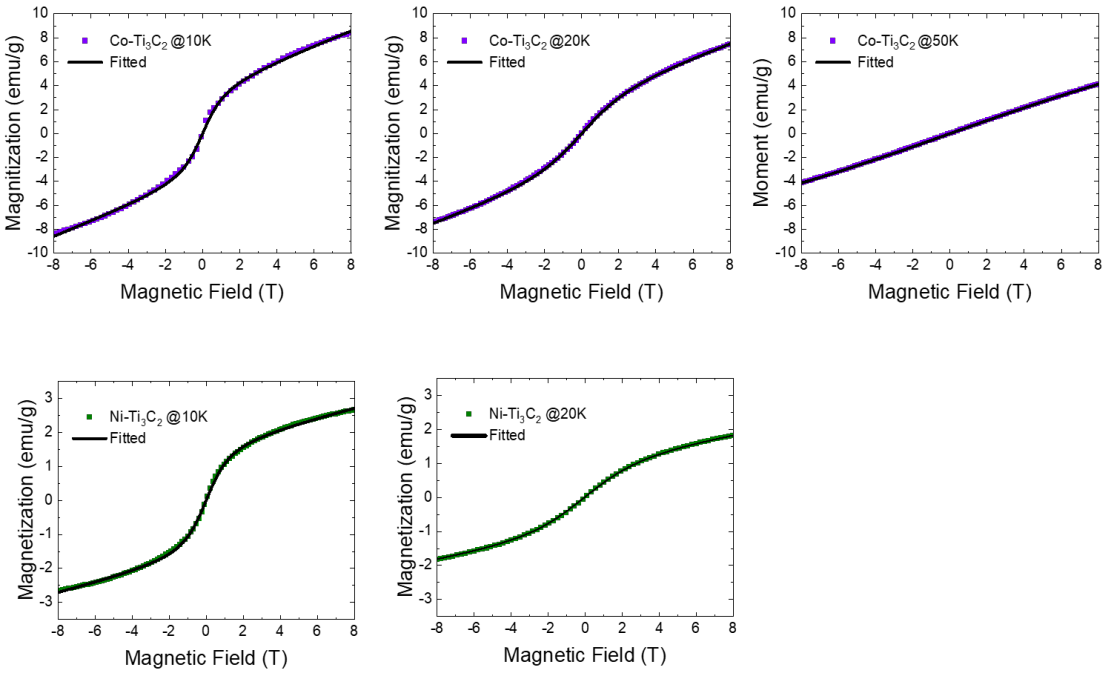

Figure S9. Magnetization as a function of magnetic field for Co-$Ti_3C_2T_x$ and Ni-$Ti_3C_2T_x$ at temperatures where non-linear behavior is observed (10 to 50 K).

Table S1. Fitting parameters for Co-$Ti_3C_2T_x$ and Ni-$Ti_3C_2T_x$ within the non-linear temperature region are shown in Fig. S9.

Sample	Temperature (K)	A (emu g^{-1})	B (J T^{-1})	C (T^{-1})
Co-$Ti_3C_2T_x$	10	1.29×10^{22}	3.03×10^{-22}	0.61
	20	1.29×10^{22}	2.71×10^{-22}	0.55
	50	1.29×10^{22}	1.71×10^{-22}	0.37
Ni-$Ti_3C_2T_x$	10	6.20×10^{21}	2.79×10^{-22}	0.14
	20	6.20×10^{21}	2.16×10^{-22}	0.09